

ARTICLE OPEN



Effect of surface modification on interfacial behavior in bioabsorbable magnesium wire reinforced poly-lactic acid polymer composites

Wahaaj Ali^{1,2}, Mónica Echeverry-Rendón¹, Alexander Kopp³, Carlos González^{1,4} and Javier LLorca^{1,4}✉

The mechanical behavior, corrosion mechanisms, and cytocompatibility at the interface of magnesium wires reinforced poly-lactic acid polymer composites were studied by in vitro degradation study of 180 days. Surface modification of Mg wires by plasma-electrolytic oxidation improved the interface shear strength from 10.9 MPa to 26.3 MPa which decreased to 8 MPa and 13.6 MPa in Mg/PLA and PEO-Mg/PLA composites, respectively, after 42 days of in vitro degradation. Cross-sections of the composite showed good cytocompatibility, although the cells tended to migrate towards the PLA regions and avoided the surface of the Mg wires. Corrosion of Mg wires (without surface modification) was very fast in composite while corrosion of surface-modified Mg wires was significantly reduced, hydrogen gas was suppressed and only 3% mass loss of Mg wires was found after 180 days. Finally, the corrosion mechanisms at interface were discussed for both composites.

npj Materials Degradation (2023)7:65; <https://doi.org/10.1038/s41529-023-00386-x>

INTRODUCTION

Bioabsorbable materials have the potential to replace conventional non-degradable metallic materials such as Ti, stainless steel, etc. in a wide range of orthopedic applications. Conventional metallic alloys provide excellent mechanical properties and biocompatibility but they remain in the body and may hinder the growth of natural tissue, an important indication in the case of children. Moreover, complications associated with the presence of a foreign element within the body (irritation of tissues, implant corrosion, loosening of the device, etc.)^{1,2} may require a second surgery for removal. Alternatively, bioabsorbable metals (such as Mg and its alloys) and polymers (such as Poly-Lactides, Poly-Glycolides, and their copolymers) have been explored in recent years^{3,4}. Poly-Lactides (PLA) are easy to process and have been used successfully for drug delivery, orthopedic implants etc.². Nevertheless, they exhibit rather long degradation times (typically years), low mechanical properties (elastic modulus = 0.35–4.14 GPa) and generate acidic by-products during degradation that can lead to an inflammatory response of the surrounding tissue⁵. Mg alloys have been used for orthopedic and cardiovascular applications in the form of fixation plates, screws, wires, stents, etc. due to their good mechanical properties (elastic modulus ~45 GPa) and biocompatibility. However, the accelerated corrosion of Mg in a physiological environment can lead to unpredictable mechanical failures, high local alkalinity, and hydrogen gas accumulation in nearby tissues^{1,6,7}.

Obviously, the combination of Mg and PLA in the form of composite materials is attractive to overcome the limitations of each other. As an example, reinforcement of PLA with Mg particles has recently shown to provide an easy route to manufacture composites by extrusion and thus enabled 3D printing of personalized scaffolds^{3,4,8}. But they accelerate the chemical and mechanical degradation of PLA during in vitro experiments and the supply of Mg²⁺ ions from composite degradation improved in vitro cytocompatibility and in vivo bone formation³, mechanical

properties could not be improved significantly⁴. Nonetheless, the reinforcement of PLA with Mg wires or fibers leads to large improvements in stiffness and strength with respect to PLA, accelerates the degradation of PLA, neutralize acidic by-products, and improves biocompatibility^{9–11}.

Further control of the degradation rate and biocompatibility of PLA reinforced with Mg wires is associated with tailoring the PLA/Mg interface through different strategies. They include treatment of the Mg reinforcement surface with hydrofluoric acid^{8,9}, saline coupling agents³, and surfactants¹² as well as electrochemical treatments by anodizing¹³ and plasma-electrolytic oxidation (PEO)^{14–16}. In fact, orthopedic fixation devices (plates and screws) of Mg modified by PEO have already shown excellent in vivo performance with enhanced bone formation around the implant^{1,6}. Therefore, using PEO surface-modified Mg wires seems promising to manufacture Mg/PLA composites for orthopedic fixation devices. To enable continuous PEO surface modification of Mg wires for use in such Mg/PLA composites, our group recently developed a continuous PEO (C-PEO) process to manufacture wires with a homogenous and porous oxide layer on the surface which showed improved mechanical, corrosion and in vitro biological performance^{7,17}. The C-PEO technique is suitable for the large-scale production of surface-modified Mg wires and is expected to improve the in vitro performance of Mg/PLA composites.

The manufacture of unidirectional Mg/PLA composites with Mg wires modified by C-PEO is reported in this paper. Since the mechanical properties and degradation rate of these bioabsorbable composites highly depend on the wire/matrix interface behavior^{18,19}, the investigation was devoted to measuring the interface shear strength of Mg/PLA and PEO-Mg/PLA composites as a function of immersion time in Simulated Body Fluid (SBF) at 37 °C by means of push-out tests^{19,20} and to study the cytocompatibility near interfacial regions by direct cell culture

¹IMDEA Materials, C/Eric Kandel 2, 28906 Getafe, Madrid, Spain. ²Department of Material Science and Engineering, Universidad Carlos III de Madrid, Leganés, Madrid 28911, Spain. ³Meotec GmbH, Philipstr. 8, 52068 Aachen, Germany. ⁴Department of Materials Science, Polytechnic University of Madrid/Universidad Politécnica de Madrid, 28040 Madrid, Spain. ✉email: javier.llorca@upm.es

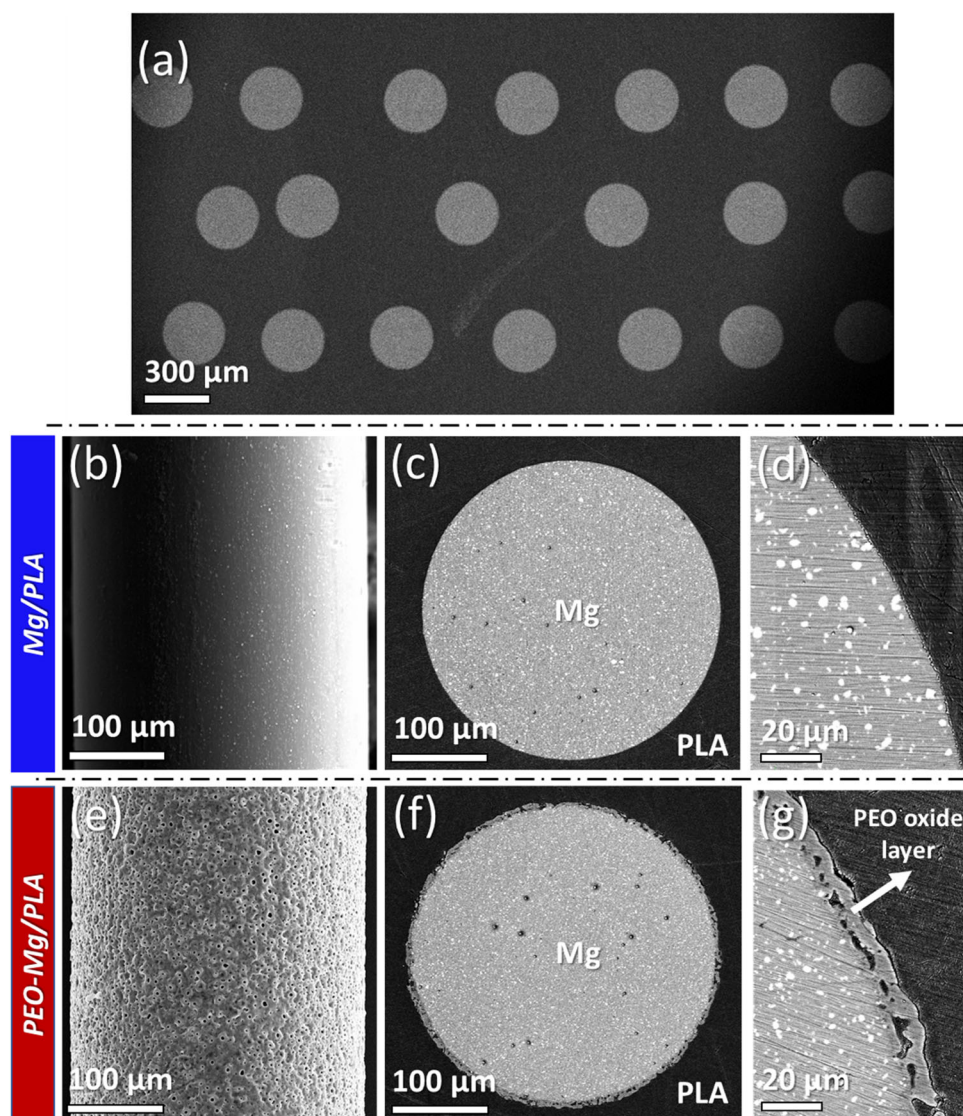


Fig. 1 Microstructure of the composites. Back-scattered electron images of (a) cross-section of the composites, (b) longitudinal surfaces of Mg wire and (c, d) cross-section of the Mg wire embedded in the PLA matrix. e Longitudinal surface of the PEO-Mg wires, and (f, g) cross-section of a PEO-Mg wire embedded in the PLA matrix.

tests. In addition, the corrosion mechanisms at the interface of the Mg wires (with and without an oxide layer introduced by PEO) and the PLA matrix were analyzed. Overall, this investigation provides the an assessment of the modification of Mg surfaces by PEO on the mechanical, corrosion, and biological behavior of Mg/PLA interfaces.

RESULTS AND DISCUSSION

Morphology of Mg/PLA and PEO-Mg/PLA interfaces

A representative cross-section of the bioabsorbable PEO-Mg/PLA composites is shown in Fig. 1a. The manufacturing method was able to obtain a fairly regular distribution of wires in the cross-section. The longitudinal surfaces of Mg and PEO-Mg wires are depicted in Fig. 1b, e, respectively. The longitudinal surfaces of Mg wires have scratches or sub-micron cracks, inevitable in the cold drawing process, while PEO-Mg wires have a porous and homogenous oxide layer produced by C-PEO¹⁷. The cross-sections of the composites (Fig. 1c–g) show that the PLA matrix is in intimate contact with the wires without any interface porosity. In the case of PEO-Mg/PLA composites, the PLA

penetrated into the pores of the PEO oxide layer (Fig. 1g). Moreover, the oxide layer was mainly composed of MgO and $\text{Mg}_3(\text{PO}_4)_2$, was not broken during processing, as confirmed by EDX in our previous study⁷.

Degradation of Mg and PEO-Mg wires inside PLA matrix

The PEO oxide layer on Mg wires had a strong effect on the in vitro degradation of the wires inside the PLA matrix. The hydrogen gas generated due to corrosion of the Mg wires in the Mg/PLA and PEO-Mg/PLA composites is plotted in Fig. 2a over the immersion time in c-SBF at 37 °C. The presence of the PEO oxide layer dramatically reduced the hydrogen gas release rate. The hydrogen release volume of Mg/PLA composites increased linearly with time during the first 100 days, followed by a plateau. After 180 days, the hydrogen volume released by Mg/PLA (60.8 ± 3.6 ml) or (7.6 ml/cm²) was ~8 times lower than that released by PEO-Mg/PLA (7.4 ± 3.5 ml) or (0.9 ml/cm²). The equivalent hydrogen gas volume normalized with respect to the original surface area of Mg wires clearly highlights the protection effect of PLA matrix and can be used to compare their corrosion rate with naked Mg wires¹⁷. Mass loss of Mg wire cores (Fig. 2b) was also estimated by image

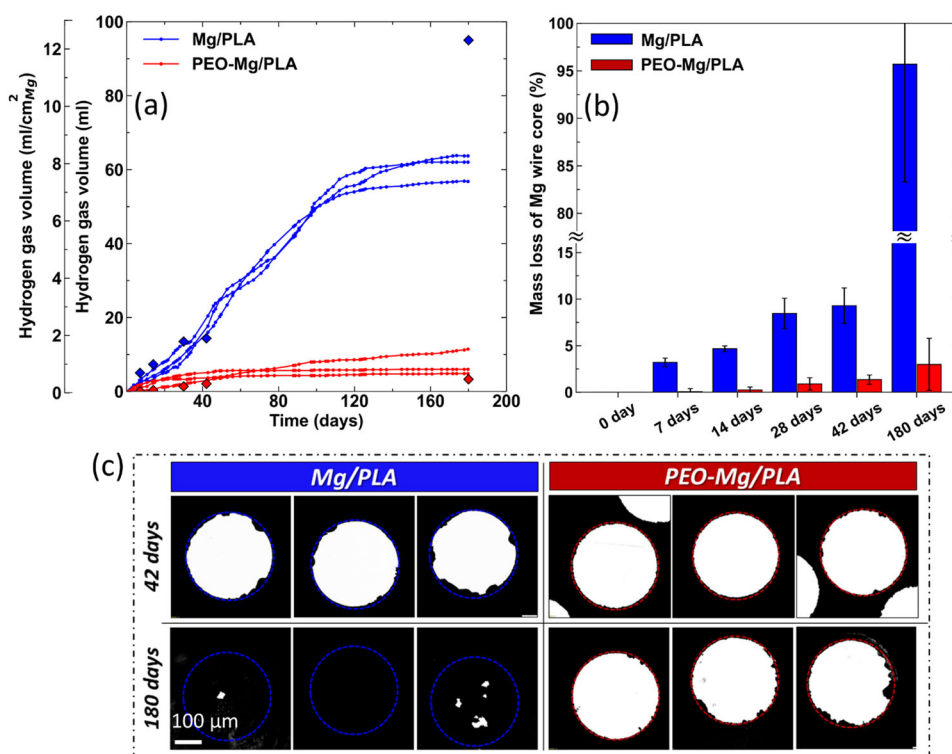


Fig. 2 Degradation of the composites in c-SBF at 37 °C. **a** Hydrogen gas evolution and **(b)** mass loss of Mg wire core estimated by image processing as a function of immersion time in c-SBF at 37 °C for Mg/PLA and PEO-Mg/PLA composites. Here, (♦) represents the hydrogen gas volume estimated by mass loss in **b** in **a** using the equation of an ideal gas. **c** Representative cross-sections of Mg wires after 42 and 180 days of degradation with and without PEO oxide layer.

processing to prove the superior performance of PEO-Mg wires inside the PLA matrix as plotted in Fig. 2a, both assuming that one atom of Mg leads to the release of one molecule of hydrogen. Representative cross-sections (Fig. 2c) confirmed that Mg wires in Mg/PLA composites corroded faster. Pit formation was evident after 42 days and Mg wires practically disappeared after 180 days. On the contrary, Mg wires in PEO-Mg/PLA suffered much less mass loss (although some pits could be observed after 180 days) due to synergetic protection provided by the oxide layer and the PLA matrix.

The estimations of hydrogen release from the image analysis of the cross-section of the Mg wires are in good agreement with hydrogen gas evolution for the whole period in the case of PEO-Mg/PLA and for the first 42 days in Mg/PLA. The total hydrogen gas volume released after 180 days in Mg/PLA was only 62% of the theoretical volume after the complete corrosion of the Mg wires. This difference, however is in agreement with previous reports^{21,22} and could be attributed to leakages or oxygen reduction reactions likely to occur during slow corrosion of Mg^{23,24}.

Degradation of PLA matrix in presence of Mg wires

DSC and GPC were used to assess the degradation of pure PLA and PLA matrix in presence of Mg wires (with and without PEO) from the glass transition temperature (T_g) and the average molecular weight (M_w), which are summarized in Table 1 for the as-manufactured condition and after 180 days in vitro degradation c-SBF at 37 °C. The short-term in vitro study (7, 14, 28, and 42 days) did not show significant changes in T_g and M_w and are not included. T_g and M_w of the as-manufactured samples decreased very slightly in the presence of Mg and PEO-Mg wires, in agreement with the previous studies that showed the addition of magnesium catalyzes the hydrolysis of PLA during high temperature processing⁴. After in vitro degradation of 180 days,

Table 1. Glass transition temperature (T_g) and average molecular weight (M_w) in the as-processed condition and after in vitro degradation of 180 days in c-SBF at 37 °C.

T_g (°C)	PLA	Mg/PLA	PEO-Mg/PLA
Time			
As-processed	55.2	49.4	50.9
180 days of degradation	55.8	42.1	44.7
M_w (g/mol) $\times 10^5$			
Time			
As-processed	4.1	3.25	3.3
180 days of degradation	2.62	0.84	1.03

T_g did not change in pure PLA coupons, but its M_w dropped, most likely due to the random chain scission of PLA oligomers triggered by hydrolytic degradation, as its mass was not changed⁵. On the contrary, the presence of Mg wires led to sharp drops in T_g and M_w to 42.1 °C and 84,000 g/mol, respectively, but the oxide layer on PEO-Mg wires reduced this drop and limited the degradation of the PLA matrix. However, it should be noted that the PLA matrix underwent localized degradation at the wire/matrix interface in the short-term degradation study (see below). The volume of polymer involved in the local degradation was insufficient to influence the GPC and DSC tests in bulk samples.

Interface shear strength

Two representative load-displacement curves of the push-out tests on Mg/PLA and PEO-Mg/PLA composites are plotted in Fig. 3a. They have the typical shape reported in the literature^{25,26}. The initial concave zone is followed by a linear region that stands for the elastic bending of the thin slice of composite in the groove of

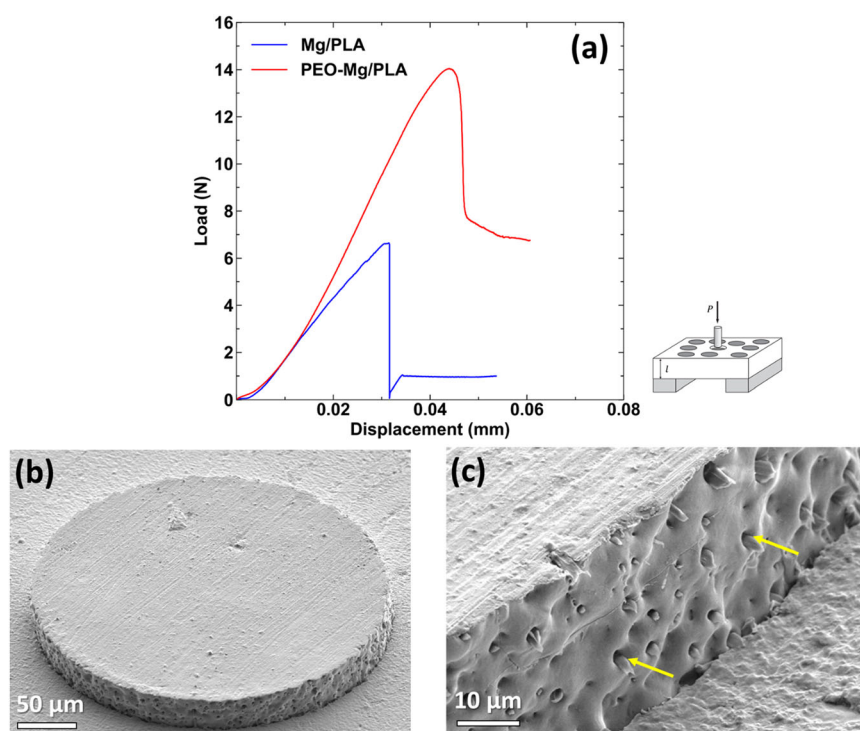


Fig. 3 Characterization of interface shear strength. **a** Representative load-displacement curves of the push-out tests in Mg/PLA and PEO-Mg/PLA composites. **b** Secondary electron image of the bottom surface of the slice after the push-out test. **c** Higher magnification view of **b** in which yellow arrows point to the ductile tearing of the PLA ligaments stuck in the pores of oxide layer.

stage. Further deformation led to the onset of non-linearity which could be attributed to the progression of a crack at wire/matrix interface, most likely from the bottom of the slice to the top (as the ratio of elastic moduli $E_{Mg}/E_{PLA} > 12^{25}$). The non-linear region ended with the complete fracture of the interface at the peak load. Afterwards, the load drops abruptly and the wire pushed out from the matrix against friction forces. The interfacial shear strengths, following Eq. (6) were 10.9 ± 1.6 MPa and 26.3 ± 1.3 MPa for Mg/PLA and PEO-Mg/PLA composites, respectively. The oxide layer created by PEO improved the interface shear strength by 2.5. This behavior was induced by the penetration of PLA into the pores of oxide layer, providing a mechanical interlock effect as confirmed in Figs. 3b, c. Fractured PLA ligaments coming out from the pores of the oxide layer are clearly seen in Fig. 3c, where ductile tearing of the PLA ligaments attached to the pores of PEO oxide layer could be observed under SEM. Finally, it should be noted that the load drop after the peak was smaller in PEO-Mg/PLA composite as compared with the Mg/PLA composite. Neither plastic deformation of the PLA matrix nor of the Mg wire was observed after the test on the top and bottom surfaces of the slice. Thus, the non-linear region in the push out curves before the peak have to be associated to the progressive crack propagation at the interface and the area under the load-displacement curves is a rough qualitative estimate the interface toughness, which was much higher in the PEO-Mg/PLA composite.

The load-displacement curves of the push-out tests on composites immersed in c-SBF during 7, 14, 28, and 42 days are plotted in Figs. 4a, b for the Mg/PLA and PEO-Mg/PLA composites, respectively. The interface shear strength (calculated from peak load before first abrupt load drop) is plotted in Fig. 4c as a function of degradation time. The interface shear strength of the Mg/PLA composite increased slightly after 7 days of immersion and then decreased up to 8.1 ± 2.1 MPa after 42 days. More interestingly, the stress necessary to push-out the wires (indicated by the plateau region after the drop from the peak load) increased with degradation time. The interface strength of the PEO-Mg/PLA

composite decreased with degradation time up to 13.6 ± 3.2 MPa after 42 days. The variation of the shear stress necessary to push-out the wires from the PLA matrix did not change with degradation time. The differences in stress necessary to push-out the wires after interface fracture between Mg/PLA and PEO-Mg/PLA can be associated with the interlock effect of the corrosion products around the wire in the former (Fig. 5a), which do not appear in the latter (Fig. 5b). Overall, the PEO oxide layer on the Mg wires improved the shear strength retention and toughness of the interface during immersion in c-SBF.

Direct cell-interface interaction

MC3T3-E1 Pre-osteoblasts were seeded on the cross-section composites for understating cell-material interaction. This information is relevant because the fabrication of customized orthopedic plates by machining can expose the Mg wires, affecting the behavior of cells near the implant. 1 h after seeding, cells are moving away from the locations occupied by the Mg wires towards the PLA, irrespective of the presence of the PEO oxide layer (Fig. 6a, b). Corrosion of Mg began as soon as it came in contact with the culture medium, leading to a near-surface increase in alkalinity and the release of hydrogen gas, and both phenomena triggered the migration of the cells to PLA regions. Cells on PLA regions could attach and proliferate rapidly, forming a monolayer to fully cover the surface after 24 h while avoiding the regions of Mg wires as shown by blue arrows in Fig. 6e, f. However, some cells migrated on regions of Mg wires after 24 h due to continuous proliferation and/or formation of passivation layer over Mg wire regions (Figs. 6e, f).

In Live/Dead assay, cells were seeded with lower density than in the proliferation experiments to clearly observe the live and dead cells after 24 h. The cells try to avoid regions of Mg wires and preferred attachment on regions of PLA matrix (Fig. 7) but some cells successfully migrated back to the Mg wires due to the formation of a passivation layer. The fraction of dead cells on the

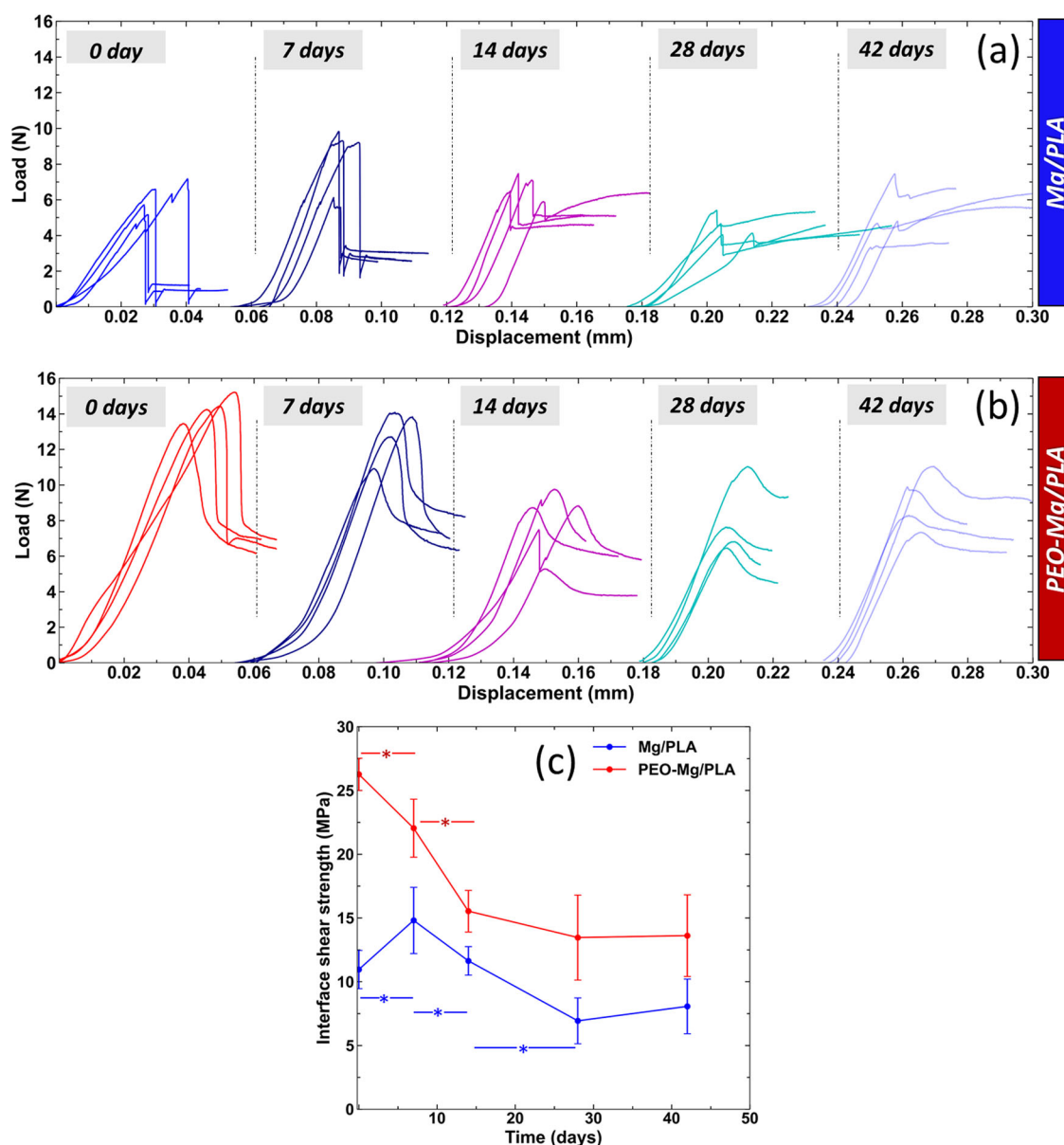


Fig. 4 Effect of immersion in c-SBF at 37 °C on interface mechanical properties. **a** Load-displacement curves of the push-out tests after 0, 7, 14, 28, and 42 days of immersion in c-SBF at 37 °C for Mg/PLA composites. **b** *Idem* for PEO-Mg/PLA composites. **c** Influence of immersion time in c-SBF on the interface shear strength. Here (*) represents $p < 0.05$ obtained by the one-way analysis of variance (ANOVA).

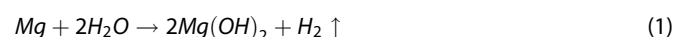
transversal cross-section is negligible, still proving the biocompatibility of the composites in general. Many cells were also found residing on edge of Mg wires (yellow circles) in order to avoid direct contact with Mg. Overall, it showed that cells are not likely to proliferate on the surface of Mg wires which is relevant for the design of Mg/PLA composite implants as the final implant shape can be achieved by either machining from a parent plate (which exposes Mg wire cross-sections to the surface) or compression in molds with the final shape. This latter strategy (in which Mg wires) are encapsulated within the PLA matrix thus seems preferable from the biocompatibility viewpoint.

Corrosion mechanisms at Mg/PLA interface

In our previous investigation, the corrosion of Mg wires (with and without PEO surface modification) directly exposed to c-SBF was analyzed in detail; see ref. ¹⁷. We concluded that—in the absence of a PEO oxide layer—localised corrosion was accelerated by the

presence of chlorine ions and led to the fast corrosion of the wires which significantly deteriorated their mechanical integrity within only 24 h. On the contrary, on PEO functionalized wires localised corrosion was suppressed by the oxide layer due to the formation of a dense corrosion layer containing O, Ca, and P beneath the PEO oxide layer, while still on top of the typical porous oxide layer resulting from the progressive oxidation of Mg to form $\text{Mg}(\text{OH})_2$. The dense corrosion layer slowed down the diffusion of chlorine ions, limiting localised corrosion and enhancing the mechanical integrity of the wires, whose strength was still above 100 MPa after 96 h in c-SBF.

In the case of the Mg/PLA composites, corrosion of Mg wires began when water molecules and chlorine ions quickly diffused (<1 day) into the PLA matrix and reached the wire surfaces. It is generally accepted that the primary corrosion reaction for magnesium involves the hydrogen evolution reaction (HER)²⁷



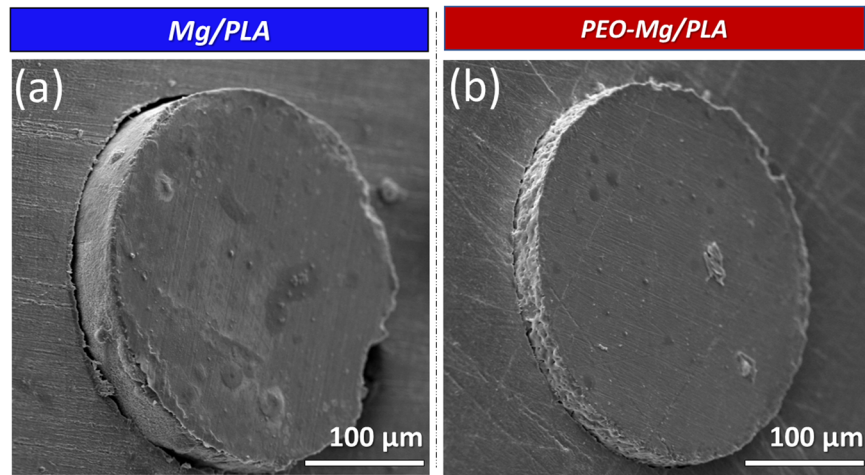


Fig. 5 **Interface fracture mechanisms.** **a, b** Secondary electron image of the bottom surface of the Mg/PLA and PEO-Mg/PLA interfaces after the push-out test after 42 days immersion in c-SBF at 37 °C.

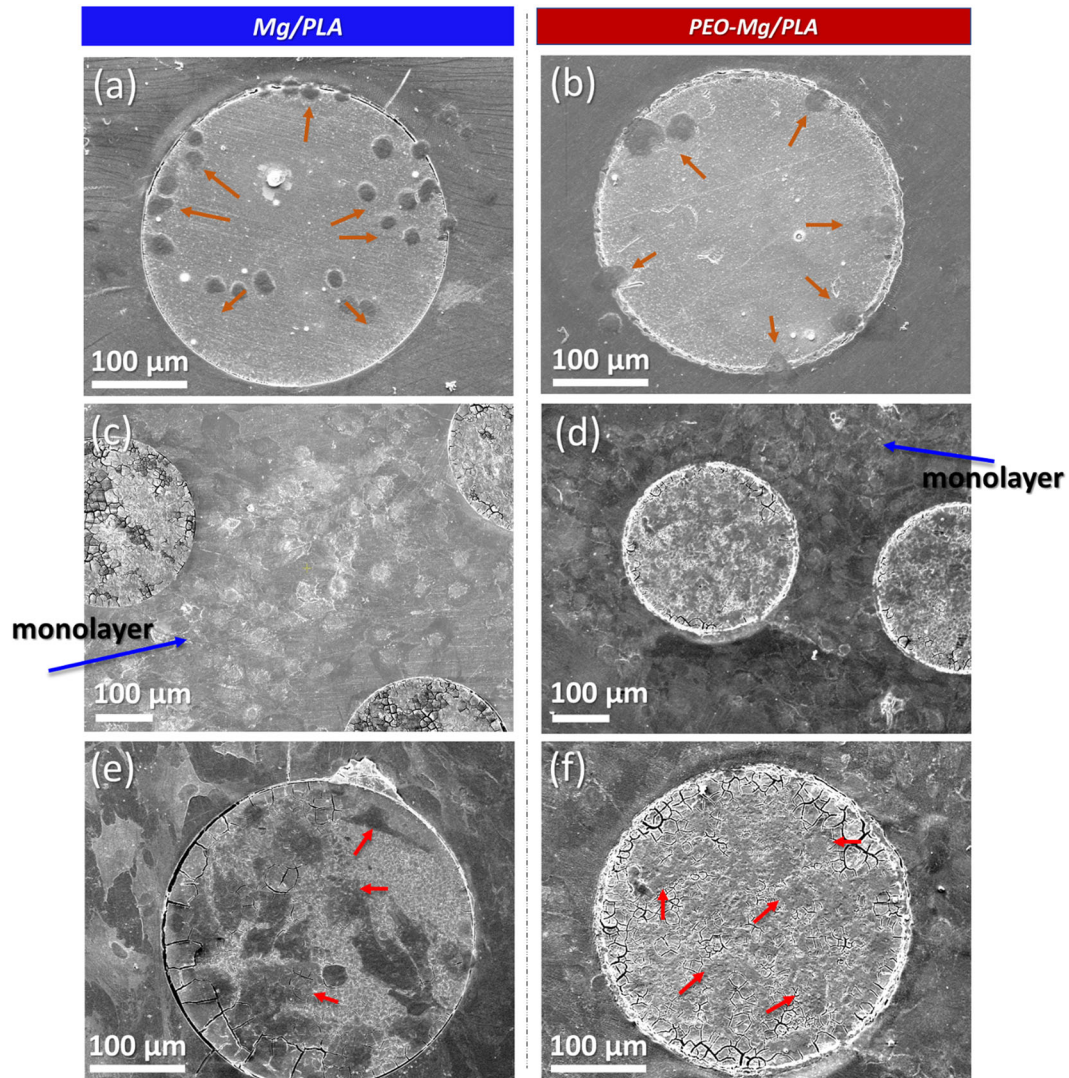


Fig. 6 **Interaction of pre-osteoblasts cells with the composite cross-sections.** **a, b** Secondary electron micrographs of MC3T3-E1 pre-osteoblasts on the cross-sectional surface of the Mg/PLA and PEO-Mg/PLA composites, respectively, after 1 h of seeding the cells. **c–f** *Idem* after 24 h of seeding the cells. Cells indicated with orange arrows tend to move away from Mg wires to PLA matrix. Thick blue arrows show the formation of a monolayer of cells between Mg wires. Red arrows show cells that are either dead or moved back to Mg wires after the formation of a passivation layer on top of the Mg wire cross-section.

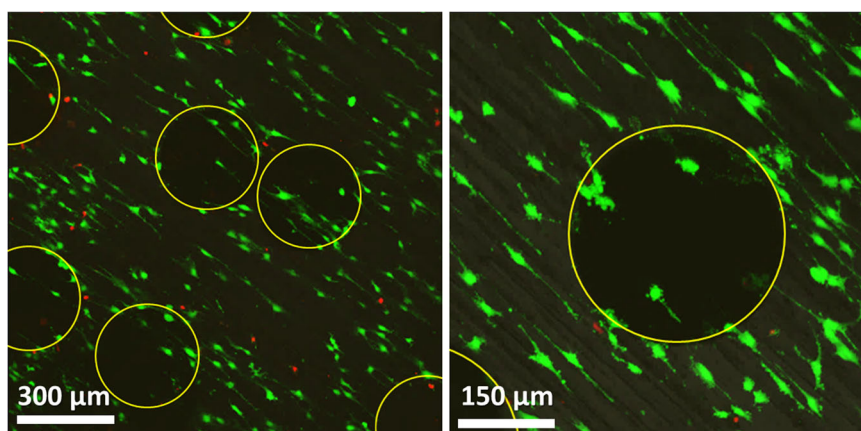


Fig. 7 Representative images of Live/Dead staining on transversal surface of PEO-Mg/PLA composite. Yellow circles show the position of wires. Cells stained in green and red are live and dead, respectively.

but the role of the oxygen reduction reaction (ORR)



cannot be ruled out, and it was pointed out recently in several studies that reported less hydrogen collection (~40%) than expected during bio-corrosion of magnesium^{21,24}. In particular, Wang et al. reported that the contribution of ORR to the total cathodic process was up to 16.5% during the slow corrosion of high-purity Mg²⁸. The limited amount of hydrogen released (as compared with the theoretical one) during the degradation of our composite samples seems to indicate that the ORR played an important role²⁹.

The $\text{Mg}(\text{OH})_2$ layer formed during corrosion can react with chlorine ions, leading to soluble MgCl_2 and OH^- ions according to

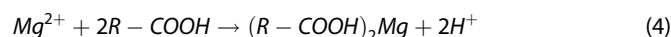


and allowing the ingress of corroding fluids to the Mg wire surface. MgCl_2 (where Mg^{2+} can be dissociated) and OH^- ions can react with the PLA by-products or diffuse outside the PLA matrix into the c-SBF solution according to several studies^{3,9,11}. As a result, the formation rate of $\text{Mg}(\text{OH})_2$ on the Mg wires was higher than the dissolution rate and a thick $\text{Mg}(\text{OH})_2$ layer was formed on the wire surface (Fig. 8a). This layer was neither dense nor continuous due to the localized chlorine attack, still allowing the progress of the wire corrosion. Moreover, the corrosion layer expanded inwards and outwards due to the increase in volume associated with the oxide formation and subjected the PLA around the wire to tensile hoop stresses. These tensile stresses were large enough to promote the cracking of PLA around wires in our previous study on the corrosion of Mg/PLA interfaces with wires of 100 μm in diameter, following a theoretical model³⁰. The same model predicts that the corrosion layer around the Mg wires of 300 μm in diameter (Fig. 8b) was not thick enough to promote PLA cracking. Instead, the interaction of OH^- ions with the polymeric chains in an alkaline environment facilitated the progressive hydrolysis and retreat of PLA at the interface.

The possible degradation mechanisms of PLA are presented in Fig. 9^{31,32}. Hydrolysis of PLA chains in neutral or acidic environments takes place by cleavage of ester bonds into two chains having carboxylic and alcohol end groups (Fig. 9a). However, PLA degrades much faster in alkaline environment³¹ which is most likely to be the cause of degradation of PLA at the interface of Mg wires because the pH can increase up to 10 near the corrosion layer of Mg^{23} . Vaid et al.³¹ reported rapid degradation of PLA fibers at a pH value of 10 compared to neutral (pH value 7.4) and acidic (pH values 2 and 3) environments. Therefore, high pH at the interface of the corrosion layer can accelerate alkali-assisted hydrolytic degradation of PLA by

possible mechanisms of intra-chain (Fig. 9b)³¹ and end-chain scissions (Fig. 9c)³². During intra-chain scission, OH^- ions hydrolyze PLA chains by randomly attacking the carbonyl group of esters, resulting in two smaller chains with an alcohol end group. While in end-chain scission, OH^- ions attack the carbonyl group nearest to the alcohol end group of PLA chain and form a six-membered lactide ring which converts into 2 molecules of lactic acid after further hydrolysis. Lactic acid is highly soluble in water and, therefore, can diffuse out of the PLA matrix and/or remain with water at the interface or in bulk PLA.

The elemental analysis by EDX along the corrosion line in Fig. 8b is plotted in Fig. 8c. It shows the presence of Mg and O, confirming the formation of $\text{Mg}(\text{OH})_2$ as a main corrosion product. Low amounts of carbon were also detected (Fig. 8d) and the concentration increased with the distance to the surface of the Mg wire, revealing the interaction of PLA degradation products with corrosion products of the Mg wires. The C source could be lactic acid, a by-product of the alkaline hydrolysis of PLA (Fig. 9b, c), or magnesium acetate formed after the reaction of Mg with $-\text{COOH}$ released by hydrolysis of PLA according to ref. ³³.



The completely corroded Mg wire inside the PLA matrix is shown in Fig. 10. The initial cross-section of the Mg wire is depicted with a dashed blue line. It shows that Mg wire expanded by the accumulation of corrosion products and the physical retreat of the PLA matrix. EDX maps confirm that corrosion products are made of $\text{Mg}(\text{OH})_2$ while there are some carbon-rich (dark) regions indicating the presence of some PLA matrix not being fully degraded. It should be noted that traces of Ca and P (that are present in c-SBF) were not found in the corrosion products of the Mg wire even after complete degradation. They are typically found in the corrosion layer when Mg wires are directly exposed to c-SBF¹⁷, but the PLA matrix stopped the penetration of Ca^{2+} and PO_4^{3-} ions towards the wire surface²⁷.

Interface shear strength between Mg wire and PLA matrix is dictated by the corrosion mechanisms at the interface. The strength increased from 10.9 MPa to 14.8 MPa after 7 days of in vitro degradation due to the accumulation of corrosion products at interface (expansion of corrosion layer) which increased the compressive normal stresses at interface. Soon, PLA also started to retreat by physical degradation due to the combination of alkali-assisted hydrolytic degradation and tensile hoop stresses. The retreat of PLA relaxed the compressive normal stresses at interface which caused the gradual reduction of interface shear strength with immersion time.

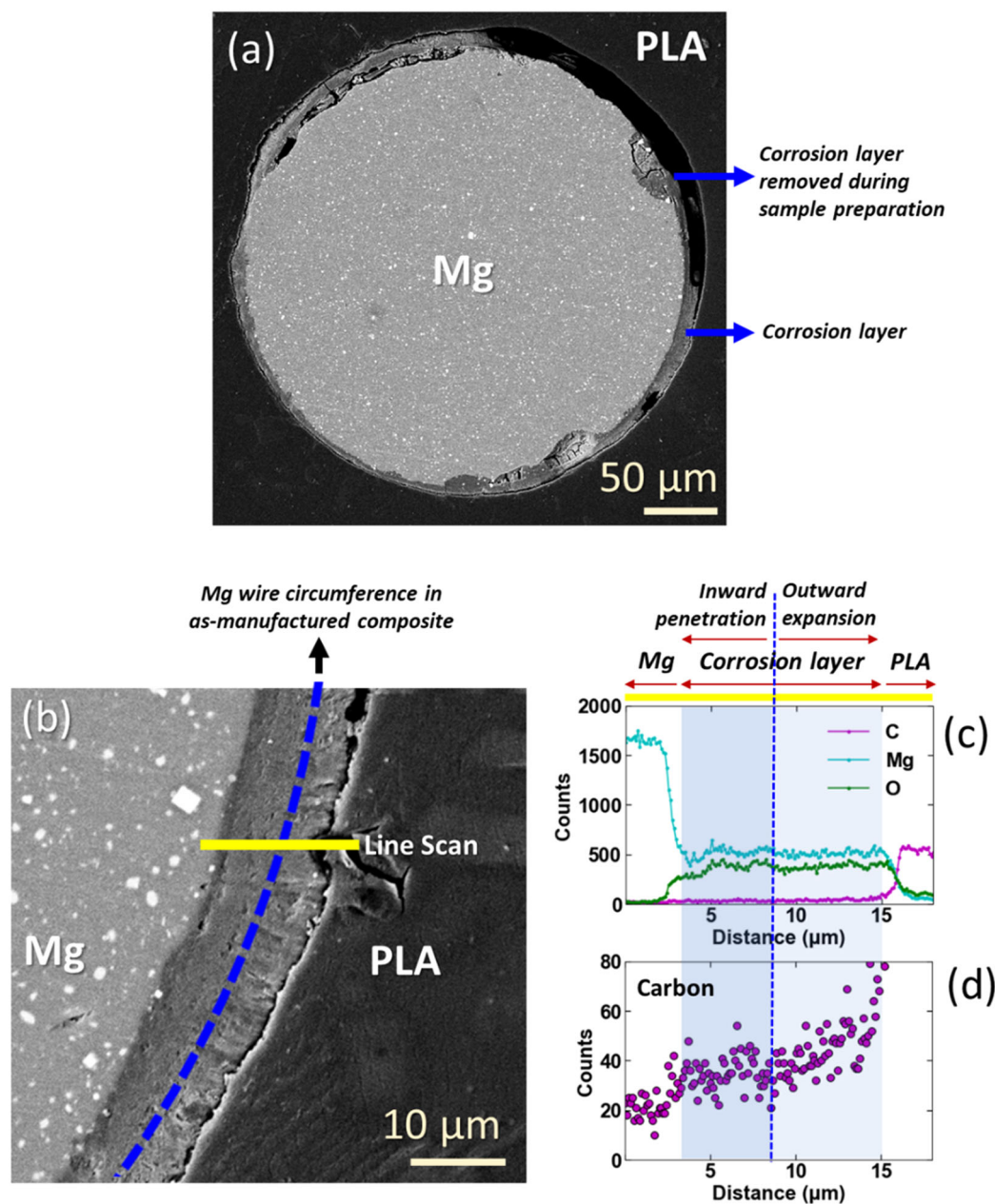


Fig. 8 Degradation mechanisms in Mg/PLA composites. Back-scattered electron images of the (a) cross-section of corroded Mg wire inside PLA matrix of composite after 42 days of in vitro degradation, (b) Detail of the corrosion layer at higher magnification. (c, d) EDX analysis along the yellow line in (b) shows the elemental composition in Mg, O, and C. The blue-shaded region shows the width of the corrosion layer.

Corrosion mechanisms at PEO-Mg/PLA interface

The corrosion mechanisms at PEO-Mg/PLA interfaces after 42 and 180 days of immersion in c-SBF are depicted in the back-scattered electron images in Figs. 11 and 12, respectively. Corrosion of the Mg wire core was very limited, even after 180 days of immersion, because corrosion products filled the cracks and pores in the PEO oxide layer and blocked the diffusion of water. The PEO oxide layer did not show corrosion after 42 days and only slight corrosion after 180 days. Since there is no corrosion layer growth outside the PEO oxide layer, the PLA matrix was not subjected to tensile stresses associated with the volumetric expansion induced by corrosion. Thus, the degradation of the PLA after 42 days of immersion was very limited (Fig. 11b) and likely to occur by alkali-assisted hydrolytic degradation (Fig. 9b, c) caused by slight corrosion of Mg wires beneath the PEO oxide layer. However, the

degradation-affected zone of the PLA matrix around the interface was noticeable after 180 days (Fig. 12a). PLA in this region became softer due to degradation and leached out during the sample preparation. Overall the physical degradation of PLA at the PEO-Mg/PLA interfaces was very mild in comparison with the Mg/PLA interfaces (Fig. 10).

The PEO oxide layer was porous and contained micro-cracks⁷; therefore, water and chlorine ions could reach the Mg wire by diffusion through the PLA matrix and pores/cracks of the oxide layer, leading to initial corrosion according to Eqs. (1)–(3). However, further corrosion of the Mg wire cores was suppressed because corrosion products filled the cracks and pores, blocking water diffusion. The PEO oxide layer did not show corrosion after 42 days and only slightly after 180 days since it is mainly composed of MgO and Mg₃(PO₄)₂ which are sparingly soluble in water and slow diffusion of water through the PLA matrix

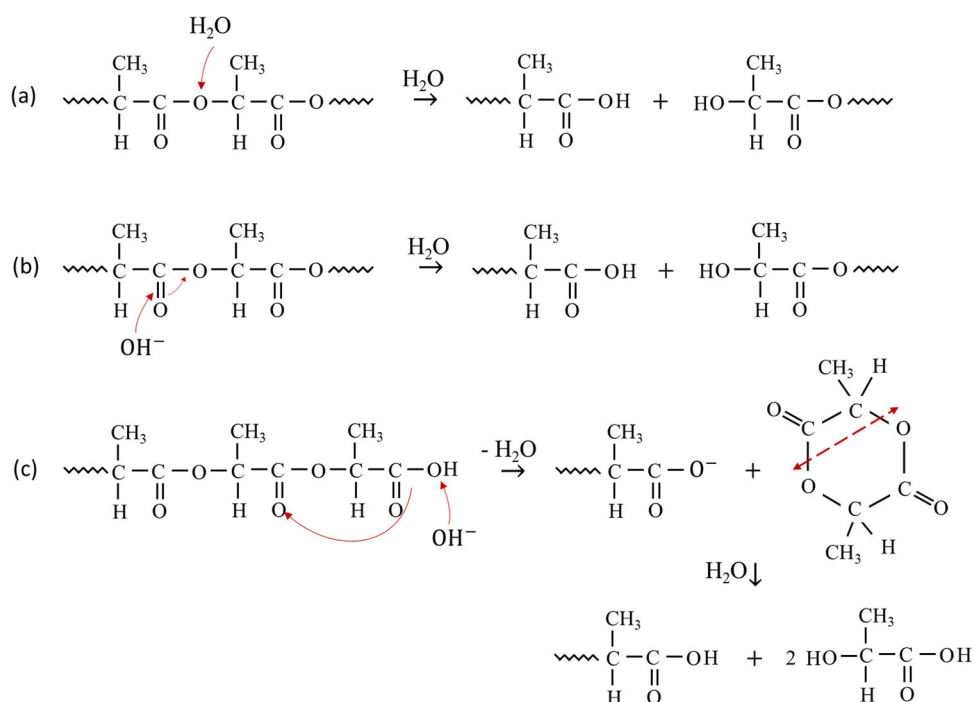


Fig. 9 Degradation processes of PLA. **a** Hydrolysis degradation of PLA in neutral and acidic environments. **b** Hydrolysis of PLA in alkaline environments through intra-chain. **c** *Idem* through end-chain attack by hydroxyl ions^{31,32}.

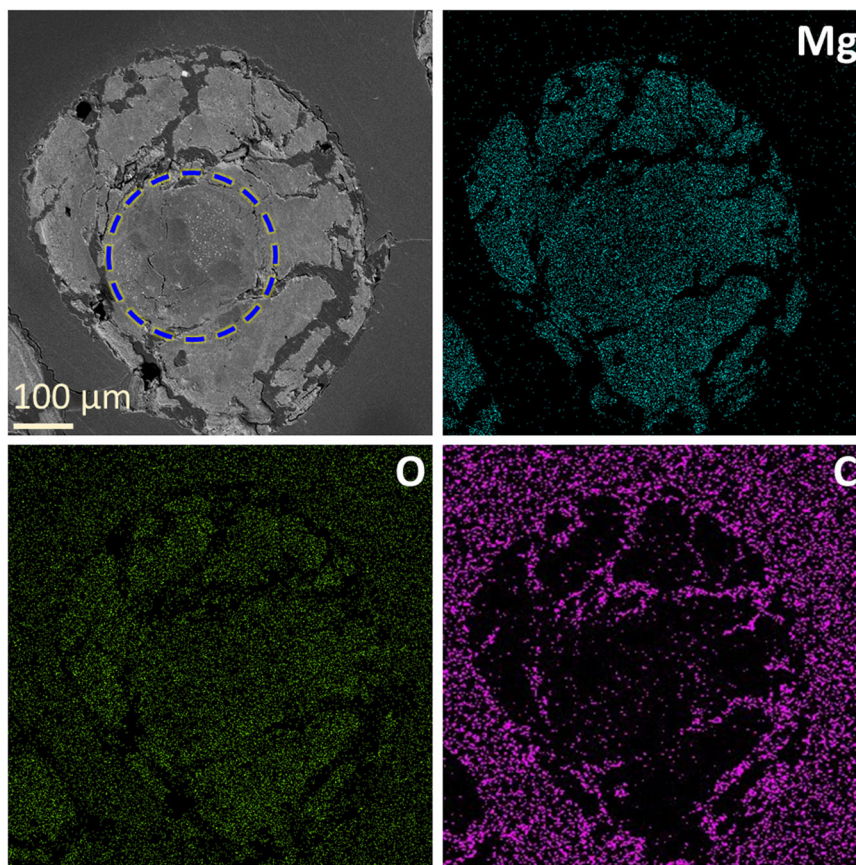


Fig. 10 Degradation of Mg wires in Mg/PLA composites. Back-scattered electron image of the cross-section of a completely corroded Mg wire in Mg/PLA composite after 180 days of in vitro degradation. The spatial distribution of Mg, O, and C obtained by EDX is plotted in the adjacent figures. The dashed blue lines indicates the initial Mg wire cross-section.

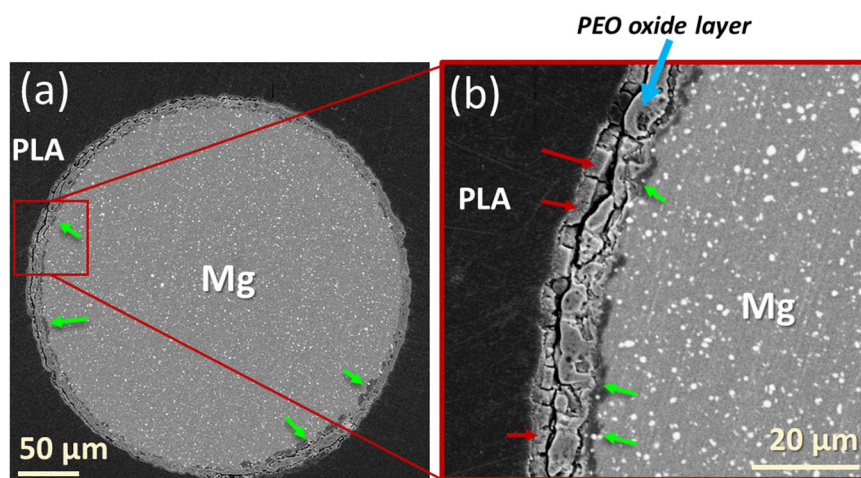


Fig. 11 Degradation mechanisms in PEO-Mg/PLA composites. **a** Back-scattered electron image of the cross-section of corroded PEO-Mg wire in PEO-Mg/PLA composite after 42 days of in vitro degradation. **b** Higher magnification image of the interface region. Red arrows show degradation of PLA matrix, while green arrows show the corrosion of Mg wires below the PEO oxide layer.

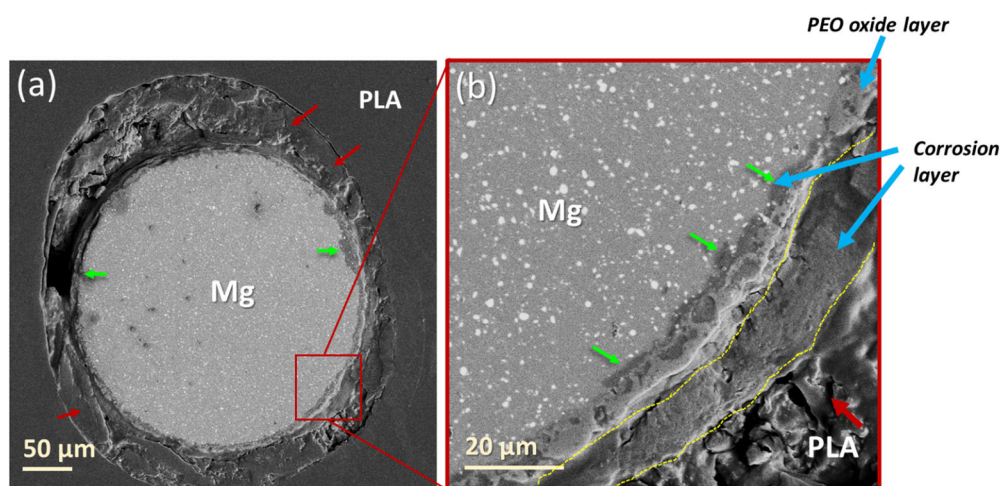


Fig. 12 Degradation mechanisms in PEO-Mg/PLA composites. **a** Back-scattered electron image of the cross-section of corroded PEO-Mg wire in PEO-Mg/PLA composite after 180 days of in vitro degradation. **b** Higher magnification image of the interface region. Red arrows show degradation of PLA matrix which was very soft and leached out during grinding process while green arrows show corrosion of Mg wires below PEO oxide layer.

provided additional protection. However, MgO is less stable than $\text{Mg}_3(\text{PO}_4)_2$ in an aqueous solution of Cl^- ions³⁴. Therefore, the corrosion of PEO oxide layer proceeded to form $\text{Mg}(\text{OH})_2$ through the reaction of MgO with water, according to ref.³⁵



This reaction disturbed the structure of the PEO oxide layer and might cause minor degradation of $\text{Mg}_3(\text{PO}_4)_2$ as shown by small traces of P in the corrosion layer (Fig. 13), but most of the PEO oxide layer remained intact (Fig. 12) since PO_4^{3-} can neither diffuse out nor penetrate in PLA matrix³⁶. The EDX maps of the interface region in Fig. 13 also confirmed the presence of P in the PEO oxide layer. At the same time, a corrosion layer was developed below the PEO oxide layer and also outwards. It was mainly formed by $\text{Mg}(\text{OH})_2$ with small traces of C and P.

Hence, the proposed corrosion mechanism also explains and confirms the trend observed in the reduction of interface shear strength of PEO-Mg/PLA composite. The strength never increased with immersion time (as opposed to the initial behavior in Mg/PLA) because the PEO oxide layer suppressed the corrosion of Mg wires and did not allow accumulation of corrosion products after

42 days (Fig. 11b). These mechanisms also indicated that the sharp drop of interface shear strength till 14 days was most likely due to the degradation of PLA present in pores of the PEO oxide layer as PLA ligaments were not observed in the pores of pushed-out wires (Fig. 5b). Afterwards, the gradual decrease of strength could be attributed to the slight physical degradation of PLA at the interface (Fig. 11b). Overall, PEO surface modification improved the interfacial performance between Mg wires and PLA matrix in as-manufactured as well as in degraded conditions by protecting the Mg wires from corrosion.

In summary, the effect of PEO surface treatment of Mg wires on the interface behavior of Mg/PLA composites was studied by means of push-out mechanical tests, in vitro degradation in simulated body fluid and direct cytocompatibility. It was found that the presence of a PEO oxide layer significantly increased the toughness and shear strength of the interface by a factor of ~2.5 due to the mechanical interlocking of PLA into the pores of the PEO oxide layer and the chemical interactions of the PLA with the oxide layer. Immersion in simulated body fluid led to a reduction in strength and toughness even though the mechanical performance of the interfaces comprising of PEO oxide layer were

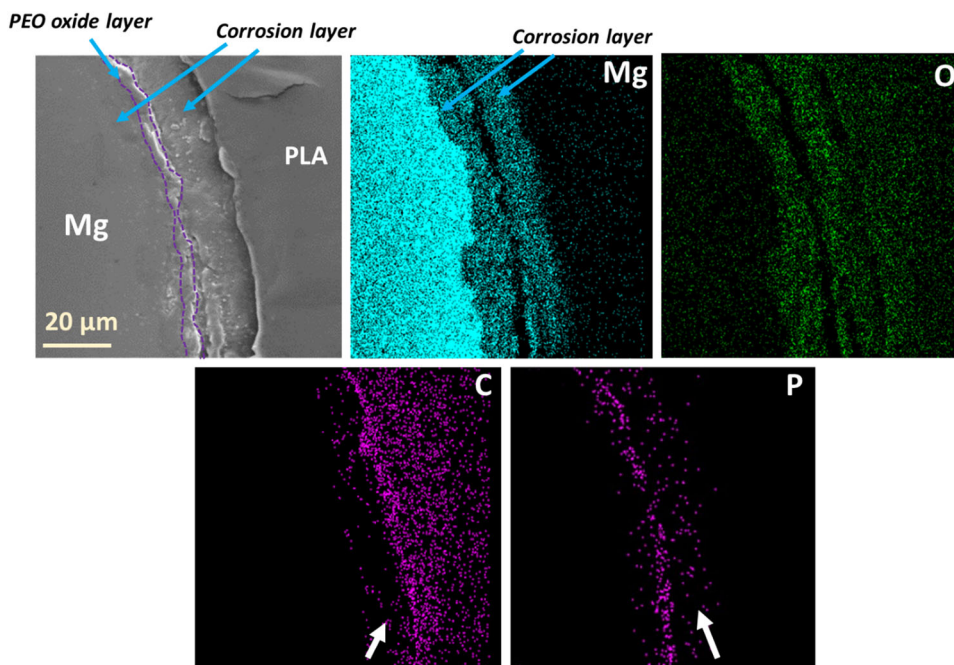


Fig. 13 Degradation mechanisms of Mg wires in PEO-Mg/PLA composites. SEM and EDS maps of enlarged view of corroded PEO-Mg wire in PEO-Mg/PLA composite after 180 days of in vitro degradation. White arrows points to traces of C and P in the corrosion layer developed outside PEO oxide layer.

always better in comparison. The proposed degradation mechanisms for both groups (Mg/PLA and PEO-Mg/PLA) explain and confirm the profound corrosion protection effect of PEO on the Mg wires during immersion in fluids, not only leading to less degradation on the Mg wires but also to less deterioration of the surrounding PLA matrix.

The trends in the degradation of interface strength were in agreement with the corrosion mechanisms observed at the interface. In the absence of a PEO oxide layer, corrosion was triggered by the degradation of the Mg wires, which led to the formation of a corrosion layer that grew inwards and outwards. At the same time, PLA retreated by physical degradation accelerated by the tensile hoop stresses induced by the expansive corrosion layer. Mg wires were completely corroded after 180 days of immersion in simulated body fluid. On the contrary, the PEO oxide layer efficiently suppressed the corrosion of Mg wires (only 3% mass loss after 180 days) and limited the degradation of the PLA matrix at the interfaces.

Direct tests as well as Live/Dead assays showed good biocompatibility of the composite cross-sections, irrespective of the presence of the PEO oxide layer. Cells migrated towards PLA regions and formed a monolayer, however avoided the surface of the Mg wires which suggests that Mg/PLA composites should be manufactured in such a way that the Mg reinforcement is preferentially fully encapsulated within the PLA matrix.

METHODS

Fabrication of Mg /PLA and PEO-Mg/PLA composites

Magnesium Y-RE-Zr alloy WE43MEO (Meotec GmbH, Aachen, Germany) with an elemental composition of 1.4–4.2% Y, 2.5–3.5% Nd, <1% (Al, Fe, Cu, Ni, Mn, Zn, Zr), and balance Mg (in wt-%) was chill-casted and wires were manufactured by indirect extrusion to produce rods with 6 mm in diameter (Meotec GmbH, Aachen, Germany) followed by successive cold drawing and annealing steps to achieve a diameter of 0.3 mm (Fort Wayne Metals Research Products Corp., Indiana, USA). The surface of the Mg wires was modified using C-PEO by passing the wire through a

phosphate-based electrolyte bath (Kermasorb®, Meotec GmbH, Aachen, Germany), facilitating process parameters as reported previously⁷. This process led to a homogeneous and porous oxide layer on the wire surface of ~8 μm in thickness. Details of the processing, microstructure, and performance of C-PEO modified Mg wires are reported into further detail in refs. ^{7,17}. Pellets of medical-grade copolymer of PLA (Purasorb PLDL 7038, Corbion, Netherlands) were used as raw material for preparing pure PLA coupons and the polymer matrix of the composites.

Composite laminae were manufactured in three steps³⁰. Firstly, unidirectional Mg wire laminae of either Mg or PEO-Mg wires (modified by C-PEO) were transferred from a spool to a plate with custom-designed winding mechanism under tension. The distance between wires was ~0.25 mm. Then, a PLA/chloroform (1 g/20 ml) slurry was poured onto the wire laminae, the chloroform evaporated and the PLA was precipitated among the wires. In the second step, PLA laminae with a thickness of 0.35 mm were prepared by hot pressing of pellets in a hot mold cavity at 220 °C and cut to the desired dimensions. In the third step, wire, and PLA laminae were alternatively stacked into a mold of 120 mm × 12 mm × 2 mm and consolidated by hot pressing at 180 °C, leading to fully dense unidirectional Mg wire reinforced PLA composites with an average wire volume fraction of 20%. In addition, PLA coupons with the same dimensions were manufactured by hot pressing of pellets.

In vitro degradation

In vitro degradation tests of the PLA, Mg/PLA, and PEO-Mg/PLA specimens were carried out at 37 °C in Simulated Body Fluid (c-SBF) with a composition (per liter) of 8.035 g NaCl, 0.355 g NaHCO₃, 0.225 g KCl, 0.231 g K₂(HPO₄)·3H₂O, 0.311 g MgCl₂·6H₂O, 0.292 g CaCl₂, 0.072 g Na₂SO₄, 6.118 g Tris base and 40 ml 1 M HCl to achieve pH of 7.4³⁶. Samples were cut to a dimension of 12 mm × 12 mm × 2 mm. Cross-sections perpendicular to the wires (where the Mg wires were exposed to the solution), were sealed with a vinyl spray coating (Full Dip, Spain) to ensure that degradation occurs by diffusion through the thickness of the sample and not by pipeline diffusion along the wire/polymer

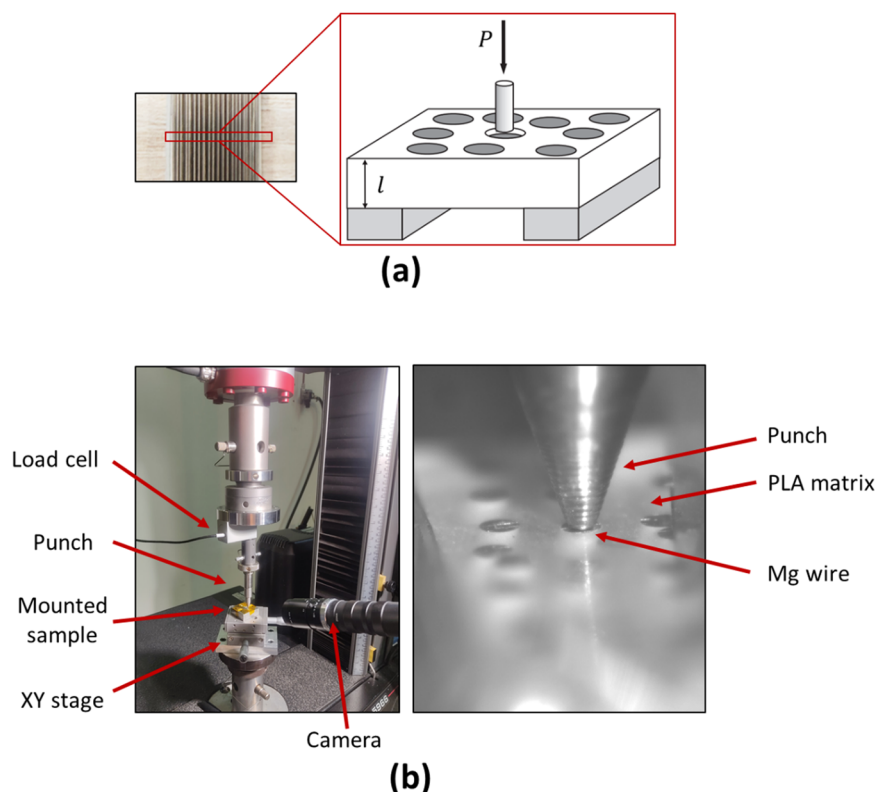


Fig. 14 Characterization of interface mechanical properties. **a** Schematic of the wire push-out test conducted on thin slices of the composites, **b** experimental setup for push-out test and enlarged image showing the punch/wire region.

interface from exposed ends. Samples were divided into short-term (7, 14, 28, and 42 days) and long-term (180 days) degradation studies and placed in a container with 200 ml of Simulated Body Fluid (c-SBF) which leads to a ratio between c-SBF volume to sample mass of $\sim 450 \text{ ml/g}$ ($>30 \text{ mL/g}$, as recommended by ISO 15814³⁷) and c-SBF volume to Mg wires surface area of 0.27 ml/mm^2 ($>0.2 \text{ ml/mm}^2$, as recommended by ASTM G31³⁸). Since there is no current standard for degradation testing of bioabsorbable metal/polymer composites such as Mg/PLA, we choose a volume of buffer solution above the minimum limits defined by both ISO 15814 (for degradation of PLA) and ASTM G31 (for corrosion of metals). Moreover, corrosion of Mg wires inside composite samples in the long-term study (180 days) was tracked by a hydrogen gas evolution setup involving glass containers, funnels, and burettes as reported in ref. ³⁹. Samples were taken from immersion medium at set time points and dried under vacuum at room temperature. The degradation mechanisms were ascertained in the scanning electron microscopy (SEM) (Apreo 25 LoVac ThermoScientific, Netherlands), using secondary and back-scattered electron modes at 10 kV after gold sputtering. Energy dispersive X-ray microanalysis (EDX) was also performed to ascertain the composition of degradation products.

Mass loss of Mg wires inside the PLA matrix was calculated by image analysis of wire cross-sections in the degraded samples. To this end, samples were extracted after in vitro study and embedded in an epoxy resin. They were grinded and polished to obtain clear images of the Mg wire in the cross-sections. Optical images (BX51 Olympus, Japan) of the wire cross sections were taken randomly. 5 and 15 images were taken from samples subjected to short-term (7, 14, 30, 42 days) and long-term degradation (180 days), respectively, and processed in ImageJ software. The area of the uncorroded regions in the Mg wire cross-sections was used to estimate the average mass loss.

Push-out tests

Wire push-out tests were performed on Mg/PLA and PEO-Mg/PLA composites to evaluate the mechanical properties at the interfaces. Intact and degraded composite samples with dimensions of $12 \text{ mm} \times 12 \text{ mm} \times 2 \text{ mm}$ were embedded in an epoxy resin (SpeciFix resin system, Struers, Denmark). They were grinded with 1200 and 4000 SiC papers to prepare thin slices of the composite (perpendicular to the wire direction) with an approximate thickness of 0.6 mm. Grinding was performed carefully from both sides of the sample (perpendicular to the wire) to use the middle section of the sample for the push-out test. Finally, both sides of samples were polished with $1 \mu\text{m}$ diamond suspension, followed by water and ethanol cleaning and drying in air.

The schematic of the experimental setup of the wire push-out test is shown in Fig. 14. Push-out tests of the wires were carried out in the thin slices that were placed on a stainless steel support with a groove of $500 \mu\text{m}$ in width. The wire to be tested was positioned manually at the center of groove with the help of an optical microscope and the slice was fixed with a tape. The support was attached to the XY stage to position the indenter punch over the desired wire. A stainless steel flat punch with $180 \mu\text{m}$ in diameter was machined in-house and fixed to the upper cross-head of an Instron Universal Testing Machine (Minneapolis, MN, USA) equipped with 100 N Instron load cell. The diameter of the flat punch was selected to minimize the plastic deformation of the Mg wire during the push-out test. The compressive load was applied on the wire under displacement control at 200 nm/s . A total of 4 and 5 wires were pushed out for each as-manufactured and degraded condition. The pushed-out wires were far away from each other to avoid any stress distortion induced by the presence of nearby pushed-out wires.

The average interfacial shear strength between the Mg wire and PLA matrix was calculated assuming full debonding according to

$$\tau = \frac{P_{\max}}{2\pi Rl} \quad (6)$$

where P_{\max} , R and l represent the maximum load recorded during the push-out test (which indicates the onset of wire sliding at the interface), the wire radius and the thickness of the composite slice, respectively. The samples were also analyzed by SEM after testing.

Thermal characterization of PLA matrix

The thermal characteristics of as-manufactured and degraded samples of the PLA coupons and composites were analyzed by differential scanning calorimetry (Q200, TA Instruments, USA) by two heating cycles performed at 10 °C/min. The glass transition temperature (T_g) from the 2nd heating cycle of DSC was used as an indicator of PLA matrix degradation because T_g values of 1st heating cycle artificially increase (in case of sample degradation) by physical aging of the polymer. The molecular weight of samples was also measured by gel permeation chromatography (GPC) (GPC 2414, Waters).

Direct cell-interface cytocompatibility

A pre-osteoblast cell line from mouse calvarial MC3T3-E1 sub-clone 4 (ATCC CRL-2593) was used to study the direct interaction of cells with the composite interfaces. Composite plates of 12 mm × 5 mm × 2 mm were cut and cross-sections showing Mg wires/PLA interfaces were grinded with 4000 SiC paper, cleaned with water and then sterilized with ethanol. Samples were placed (perpendicular to the wire direction) in 24 well-plate and alpha-MEM medium (Invitrogen, USA) supplemented with 10% Fetal Bovine Serum (FBS) (Invitrogen, USA) and 1% penicillin/streptomycin (Invitrogen, USA) containing MC3T3-E1 pre-osteoblast cells was added directly to the wells. The cell concentration was kept at 20,000 cells/cm² and 10,000 cells/cm² for SEM and Live/Dead assays, respectively. Afterwards, the plate was maintained at 37 °C in a humidified 5% CO₂ atmosphere. Cell morphology was observed by SEM after 1 h and 24 h. Cells were washed with DPBS and fixed to the surface of samples with 4% PFA solution for 15 min. Afterwards, cells were dehydrated by serial immersion in ethanol/H₂O solutions with increasing concentration (30%, 50%, 70, 80%, 90%, and 100%) of ethanol for 10 min each and analyzed by SEM to study cell attachment. Cell behavior at interfacial regions was also assessed by Live/Dead assay (Invitrogen, USA). Culture medium was removed after 24 h incubation of cells on the cross-sectional surface of samples and then samples were washed by DPBS solution (with Ca and P). Then staining solution of DPBS (with Ca and P) (Gibco) containing 4 μM Calcein-AM and 2 μM Ethidium homodimer-1 was added to plates followed by incubation for 20 min at 37 °C. Finally, samples were inverted and imaged under a confocal microscope (Olympus FV3000, Japan).

DATA AVAILABILITY

The data that support the findings of this study are available on request from the corresponding author.

Received: 30 April 2023; Accepted: 28 July 2023;

Published online: 10 August 2023

REFERENCES

- Rendenbach, C. et al. Improved in vivo osseointegration and degradation behavior of PEO surface-modified WE43 magnesium plates and screws after 6 and 12 months. *Mater. Sci. Eng. C* <https://doi.org/10.1016/j.msec.2021.112380> (2021).
- Pina, S. & Ferreira, J. Bioresorbable plates and screws for clinical applications: a review. *J. Healthc. Eng.* **3**, 243–260 (2012).
- Yu, X. et al. Study of engineered low-modulus Mg/PLLA composites as potential orthopaedic implants: an in vitro and in vivo study. *Colloids Surf. B Biointerfaces* **174**, 280–290 (2019).
- Pascual-González, C. et al. Processing and properties of PLA/Mg filaments for 3D printing of scaffolds for biomedical applications. *Rapid Prototyp. J.* **28**, 884–894 (2022).
- Buchanan, F. *Degradation Rate Of Bioresorbable Materials, Prediction And Evaluation* (Woodhead Publishing Limited, 2008).
- Kopp, A. et al. Long-term in vivo observations show biocompatibility and performance of ZX00 magnesium screws surface-modified by plasma-electrolytic oxidation in Göttingen miniature pigs. *Acta Biomater.* **157**, 720–733 (2023).
- Ali, W. et al. Bioabsorbable WE43 Mg alloy wires modified by continuous plasma-electrolytic oxidation for implant applications. Part I: processing, microstructure and mechanical properties. *Biomater. Adv.* **146**, 213314 (2023).
- Wan, P., Yuan, C., Tan, L. L., Li, Q. & Yang, K. Fabrication and evaluation of bioresorbable PLLA/magnesium and PLLA/magnesium fluoride hybrid composites for orthopedic implants. *Compos. Sci. Technol.* **98**, 36–43 (2014).
- Ali, W., Mehboob, A., Han, M. G. & Chang, S. H. Effect of fluoride coating on degradation behaviour of unidirectional Mg/PLA biodegradable composite for load-bearing bone implant application. *Compos. Part A Appl. Sci. Manuf.* **124**, 105464 (2019).
- Li, X. et al. Degradation behaviors of Mg alloy wires/PLA composite in the consistent and staged dynamic environments. *Mater. Sci. Eng. C* **103**, 109765 (2019).
- Cai, H. et al. In vitro study on cytocompatibility of Mg wire/poly(lactic acid) composite rods. *J. Mater. Eng. Perform.* <https://doi.org/10.1007/s11665-021-05883-1> (2021).
- Ferrandez-Montero, A., Lieblich, M., Benavente, R., González-Carrasco, J. L. & Ferrari, B. New approach to improve polymer-Mg interface in biodegradable PLA/Mg composites through particle surface modification. *Surf. Coat. Technol.* **383**, 125285 (2020).
- Butt, M. S. et al. Mechanical and degradation properties of biodegradable Mg strengthened poly-lactic acid composite through plastic injection molding. *Mater. Sci. Eng. C* **70**, 141–147 (2017).
- Li, X. et al. Biodegradable poly-lactic acid based-composite reinforced unidirectionally with high-strength magnesium alloy wires. *Biomaterials* **49**, 135–144 (2015).
- Cai, H. et al. Enhanced fully-biodegradable Mg/PLA composite rod: Effect of surface modification of Mg-2Zn wire on the interfacial bonding. *Surf. Coat. Technol.* **350**, 722–731 (2018).
- Cai, H. et al. Insight into the effect of interface on the mechanical properties of Mg/PLA composite plates. *Compos. Sci. Technol.* **183**, 107801 (2019).
- Ali, W. et al. Bioabsorbable WE43 Mg alloy wires modified by continuous plasma-electrolytic oxidation for implant applications. Part II: degradation and biological performance. *Biomater. Adv.* **147**, 213325 (2023).
- Ananth, C. R. & Chandra, N. Evaluation of interfacial shear properties of metal matrix composites from fibre push-out tests. *Mech. Compos. Mater. Struct.* **2**, 309–328 (1995).
- González, C. & Llorca, J. Micromechanical modelling of deformation and failure in Ti-6Al-4V/SiC composites. *Acta Mater.* **49**, 3505–3519 (2001).
- Collard, B., Giuliani, F., Ingenbleek, G., Verbiest, G. & Dini, D. A fracture mechanics analysis of the micromechanical events in finite thickness fibre push-out tests. *Theor. Appl. Fract. Mech.* **121**, 103441 (2022).
- Kirkland, N. T., Birbilis, N. & Staiger, M. P. Assessing the corrosion of biodegradable magnesium implants: a critical review of current methodologies and their limitations. *Acta Biomater.* **8**, 925–936 (2012).
- Li, M. et al. Microstructure, mechanical properties, corrosion resistance and cytocompatibility of WE43 Mg alloy scaffolds fabricated by laser powder bed fusion for biomedical applications. *Mater. Sci. Eng. C* **119**, 111623 (2021).
- Wang, C., Xu, W., Höche, D., Zheludkevich, M. L. & Lamaka, S. V. Exploring the contribution of oxygen reduction reaction to Mg corrosion by modeling assisted local analysis. *J. Magnes. Alloy.* <https://doi.org/10.1016/j.jma.2022.09.031> (2022).
- Mei, D., Lamaka, S. V., Lu, X. & Zheludkevich, M. L. Selecting medium for corrosion testing of bioabsorbable magnesium and other metals – A critical review. *Corros. Sci.* **171**, 108722 (2020).
- Bechel, V. T. & Sottos, N. R. Application of debond length measurements to examine the mechanics of fiber pushout. *J. Mech. Phys. Solids* **46**, 1675–1697 (1998).
- Schönen, S. et al. Insight into single-fiber push-out test of tungsten fiber-reinforced tungsten. *Compos. Interfaces* **26**, 107–126 (2019).
- Dai, J. et al. Poly-lactic acid coatings on the biomedical WE43 Mg alloy: Protection mechanism and ion permeation effects. *Prog. Org. Coat.* **177**, 107427 (2023).
- Wang, C. et al. High rate oxygen reduction reaction during corrosion of ultra-high-purity magnesium. *npj Mater. Degrad.* **4**, 1–5 (2020).
- Zeller-plumhoff, B., Akkineni, A. R. & Mosshammer, M. Oxygen-sensitive nanoparticles reveal the spatiotemporal dynamics of oxygen reduction during

- magnesium implant biodegradation. *npj Mater. Degrad.* <https://doi.org/10.1038/s41529-022-00302-9> (2022).
30. Ali, W., Echeverry-Rendón, M., Kopp, A., González, C. & LLorca, J. Strength, corrosion resistance and cellular response of interfaces in bioresorbable poly-lactic acid/Mg fiber composites for orthopedic applications. *J. Mech. Behav. Biomed. Mater.* **123**, 104781 (2021).
 31. Vaid, R., Yildirim, E., Pasquinelli, M. A. & King, M. W. Hydrolytic degradation of polylactic acid fibers as a function of pH and exposure time. *Molecules* **26**, 7554 (2021).
 32. Koterwa, A. et al. The role of electrolysis and enzymatic hydrolysis treatment in the enhancement of the electrochemical properties of 3D-printed carbon black/poly(lactic acid) structures. *Appl. Surf. Sci.* **574**, 151587 (2022).
 33. Cai, H. et al. In vitro degradation behavior of Mg wire/poly(lactic acid) composite rods prepared by hot pressing and hot drawing. *Acta Biomater.* <https://doi.org/10.1016/j.actbio.2019.05.059> (2019).
 34. Lu, X. et al. Degradation behavior of PEO coating on AM50 magnesium alloy produced from electrolytes with clay particle addition. *Surf. Coat. Technol.* **269**, 155–169 (2015).
 35. Zeng, R. C. et al. In vitro corrosion and cytocompatibility of a microarc oxidation coating and poly(l-lactic acid) composite coating on Mg-1Li-1Ca alloy for orthopedic implants. *ACS Appl. Mater. Interfaces* **8**, 10014–10028 (2016).
 36. Oyane, A. et al. Preparation and assessment of revised simulated body. *J. Biomed. Mater. Res. - Part A* **65A**, 188–195 (2003).
 37. ISO 15814:1999 Implants for surgery — Copolymers and blends based on polylactide — In Vitro degradation testing. (1999).
 38. ASTM G31-72: *Standard Practice for Laboratory Immersion Corrosion Testing of Metals*. (2004).
 39. Song, G. L. 1 - *Corrosion electrochemistry of magnesium (Mg) and its alloys. Corrosion of Magnesium Alloys* (Woodhead Publishing Limited, 2011).

ACKNOWLEDGEMENTS

This investigation was supported by the European Union's Horizon 2020 research and innovation program under the European Training Network Biolmplant (Development of improved bioabsorbable materials for orthopedic and vascular implant applications), Marie Skłodowska-Curie grant agreement No 813869. Additional support from the Spanish Research Agency through the grant PID2021-124389OB-C21 is also gratefully acknowledged.

AUTHOR CONTRIBUTIONS

W.A. carried out the experiments reported in this paper. M.E. designed and supervised the biological experiments. C.G. and J.L.L. designed and supervised the investigation. W.A. and J.L.L. wrote the original draft. All authors edited the original draft and participated in the elaboration of the final manuscript.

COMPETING INTERESTS

A.K. is employed by Meotec GmbH. Presented Mg/PLA composites are in development and commercially not available. The authors declare no conflict of interests.

ADDITIONAL INFORMATION

Correspondence and requests for materials should be addressed to Javier LLorca.

Reprints and permission information is available at <http://www.nature.com/reprints>

Publisher's note Springer Nature remains neutral with regard to jurisdictional claims in published maps and institutional affiliations.



Open Access This article is licensed under a Creative Commons Attribution 4.0 International License, which permits use, sharing, adaptation, distribution and reproduction in any medium or format, as long as you give appropriate credit to the original author(s) and the source, provide a link to the Creative Commons license, and indicate if changes were made. The images or other third party material in this article are included in the article's Creative Commons license, unless indicated otherwise in a credit line to the material. If material is not included in the article's Creative Commons license and your intended use is not permitted by statutory regulation or exceeds the permitted use, you will need to obtain permission directly from the copyright holder. To view a copy of this license, visit <http://creativecommons.org/licenses/by/4.0/>.

© The Author(s) 2023